Buoyancy-Driven Flow and Nature of Vertical Mixing in a Zonally Averaged Model

Olivier Marchal[1], Charles Jackson[2], Johan Nilsson[3], André Paul[4], and Thomas F. Stocker[5]

The consequences for the meridional overturning circulation (MOC) of fundamentally different assumptions about the vertical effective diffusivity of heat and salt (κ_v) are examined in a zonally averaged model of the buoyancy-driven flow in one- and two-hemisphere basins. First, we replicate results obtained in earlier studies from a zonally averaged model based on a less elaborate closure for the zonal pressure difference. For a single-hemisphere basin, the equilibrium response of the MOC to freshwater forcing (salt addition at low latitudes and salt extraction at high latitudes) depends qualitatively on the nature of vertical mixing: if the diffusivity is constant (a common assumption), the MOC decreases with increased forcing, whereas if it depends on vertical density stratification (at least an equally plausible assumption) the MOC increases with increased forcing. For a two-hemisphere basin, on the other hand, the equilibrium response of the MOC in the dominant hemisphere to increased freshwater forcing (symmetric about the equator) is an amplification for both mixing representations. Second, we investigate the instability of the flow at large freshwater forcing. For both basins, the flow is more stable to the forcing if κ_v varies with vertical stratification. For a single-hemisphere basin, self-sustained oscillations of the flow that are quasi-periodic (e.g., millennial) are found for both fixed and stability-dependent κ_v. For a two-hemisphere basin, such oscillations are found only when κ_v is stability-dependent. For both basins, the occurrence and period of the oscillations are partly determined by the energy available for vertical mixing if κ_v varies with vertical stratification. A possible analogy with the relaxation oscillations of van der Pol is presented.

1. INTRODUCTION

Fluid flows are often so complicated that laboratory experiments or the numerical solution of the equations of motion are the only route to simulate their behavior in natural circumstances. With the advent of modern computers, numerical models have become an indispensable tool to simulate geophysical flows, such as the general circulation of the ocean. Numerical models of the ocean circulation have diverse merits, such as (i) their capability to represent terms in the equations of motion that are often neglected in analytical work (the non-linear advection terms are a prominent example), (ii) their ability to accommodate complex initial and boundary conditions, and (iii) their capability to incorporate realistic basin geometries. Their scientific and societal values can be justified on various grounds. In particular,

[1]Department of Geology and Geophysics, Woods Hole Oceanographic Institution, Massachusetts, USA.
[2]Institute of Geophysics, University of Texas at Austin, USA.
[3]Department of Meteorology, University of Stockholm, Sweden.
[4]Department of Geosciences, University of Bremen, Germany.
[5]Climate and Environmental Physics Division, Physics Institute, University of Bern, Switzerland.

Ocean Circulation: Mechanisms and Impacts
Geophysical Monograph Series 173

10.1029/173GM05

they can be used to explore the sensitivity to external perturbations of the meridional overturning component of the general circulation—the meridional overturning circulation or MOC—which is thought to play an important role in climate owing to the associated meridional flux of heat (e.g., *Bryden and Imawaki* [2001]).

The solution of the equations of fluid motion on a grid implies that sub-grid scale phenomena are omitted or at best parameterized. Obvious oceanographic examples are the transports of momentum, heat, and salt at the scales that are smaller than the horizontal and vertical spacings of the grid. The range of spatial scales that characterize the unresolved transports is huge. Current models of the ocean general circulation have grids with a horizontal spacing of $O(10^4)$ m to $O(10^5)$ m and a vertical spacing of $O(10^1)$ m to $O(10^3)$ m. In contrast, the molecular diffusivities of momentum ($\sim 10^{-6}$ m^2 s^{-1}), heat (10^{-7} m^2 s^{-1}), and salt in seawater (10^{-9} m^2 s^{-1}) are so small that the frictional dissipation and the actual mixing of water properties become only effective at scales of $O(10^{-3})$ m to $O(10^{-2})$ m. Between the scales that are resolved by the models and the scales at which these variables are dissipated is a range of transport phenomena whose proper representation in models of the large-scale flow remains one of the most vexing problems in geophysical fluid dynamics [*Pedlosky*, 1987].

A common assumption in numerical models of the ocean general circulation is that the unresolved small-scale motions operate effectively on the resolved large-scale motions as Fickian diffusion, with diffusivities that are several orders of magnitude larger than those for molecular diffusion (a Reynolds decomposition of the dynamical equations has led to various terminologies, e.g., 'turbulent' or 'eddy' diffusivities). Thus, the flux of variables such as momentum, heat, and salt is assumed to be proportional to the gradient of these variables computed at the grid points, the direction of the flux being downgradient. The representation of small-scale transport phenomena as diffusion raises two legitimate questions: (i) is the representation accurate? and (ii) assuming that it is accurate, which values of the effective diffusivities should be used in the numerical integrations? Whether the representation is accurate remains unclear, as there appears to be no observational evidence that the transport of momentum, heat, and salt at small scales operates effectively as diffusion on large scales. Tests of the representation from results obtained with eddy-resolving models are a subject of ongoing research. Which values to use for the effective diffusivities is equally problematic. Such values are constrained on the basis of (i) observational estimates (when available), (ii) values used in earlier numerical studies; (iii) a comparison a posteriori between the modeled and observed distributions of water properties such as temperature (T) and salinity (S); and/or (iv) a stability criterion that must be met by the numerical method used to integrate the equations of motion. In many cases, option (iii) is an important guide, which implies the fundamental difficulty of truly testing numerical models given that T, S measurements often compose most of the available data base.

Among the motions that are unresolved by the coarsest resolution models are mesoscale eddies (with horizontal scales of $O(10^4)$ m). Although higher resolution models can simulate eddying motions, they remain too expensive computationally for use in the long-term integrations that are needed in climate studies. Thus, eddies need to be parameterized. For example, *Gent and McWilliams* [1990] developed a parameterization scheme for the transport of heat and salt by eddies in coarse resolution models. In this scheme, the transport by eddies is represented as an additional velocity with components that are proportional to the spatial variations of the local isopycnal slope, the coefficient of proportionality being called the 'thickness diffusivity' [*Gent et al*., 1995].

Here it is assumed that the representation of the sub-grid scale transports as Fickian diffusion is formally accurate, following the vast majority of earlier numerical studies of the large-scale circulation. Thus, we focus on the second question raised above, more specifically on the effective diffusivities for the vertical transport of heat and salt (hereafter these diffusivities are generically referred to as κ_v, a vertical diffusivity for buoyancy). Small-scale vertical mixing in the ocean interior (i.e., away from boundary layers and fronts) is thought to be dominated by the breaking of internal waves. Formal discussions of this phenomenon are often centered around a postulated balance between (i) the production of turbulent kinetic energy (TKE) by the vertical shear in the mean flow, (ii) the vertical turbulent flux of buoyancy, and (iii) the viscous dissipation of TKE. The balance can be expressed succinctly as

$$\kappa_v = \frac{R_f}{1 - R_f} \frac{\varepsilon}{N^2}. \tag{1}$$

Here R_f is the flux Richardson number, ε is the rate of dissipation of TKE, and N is the buoyancy frequency (for the various assumptions leading to (1) see, e.g., *Osborn* [1980]). Importantly, (1) suggests that the diffusivity may depend on local stratification, although the nature of this dependence is not well established. For example, models of dissipation in an internal wave field imply different scalings of ε versus N and thus different scalings of κ_v versus N [*Polzin et al*., 1995]. Thus, significant uncertainties remain regarding the nature of the dependence of κ_v on local stratification in the ocean interior.

The dynamical implications of different assumptions about vertical mixing have been appreciated in several studies

(e.g., *Gargett* [1984]; *Cummins et al*. [1990]; *Hu* [1996]; *Huang* [1999]). In particular, models of the buoyancy-driven flow in a single-hemisphere basin have been used to explore the equilibrium response of the MOC to changes in surface buoyancy forcing for different assumptions about κ_v [*Nilsson and Walin*, 2001; *Nilsson et al*., 2003; *Mohammad and Nilsson*, 2004]. If κ_v is constant (a diffusivity that does not depend explicitly on stratification is a common assumption in circulation models), the strength of the MOC decreases with increased freshwater forcing—the forcing being defined as the contrast between surface freshwater removal at low latitudes and surface freshwater supply at high latitudes—whereas if κ_v is stability-dependent (at least an equally plausible assumption) the opposite result holds [*Nilsson and Walin*, 2001; *Mohammad and Nilsson*, 2004]. Thus, the equilibrium response of the MOC to perturbations in the surface buoyancy forcing is *qualitatively* dependent on the representation of vertical mixing in the models.

This result is important, for it appears to challenge a hypothesis of climate change, whereby a freshening of surface waters in the northern North Atlantic would cause a reduction in the strength of the MOC and in the associated poleward heat flux. This view emerged in large part from simulations with a hierarchy of ocean models (sometimes coupled with atmospheric models) which, however, share a common assumption: κ_v does not depend on vertical density stratification. In an ocean where κ_v is stability-dependent, the vertical diffusion of buoyancy is not constant but changes with the circulation, which provides a feedback on the response of the MOC to perturbations in surface buoyancy forcing. The aforementioned studies illustrated that the feedback can change the sign of the response of the MOC to freshwater forcing. An outstanding question is whether this feedback could operate in the real ocean.

In this paper we investigate the dynamical effects of a stability-dependent κ_v in a zonally averaged model of the buoyancy-driven flow in one- and two-hemisphere basins. Scaling arguments [*Saenko and Weaver*, 2003] and a numerical study with a zonally averaged model [*Mohammad and Nilsson*, 2006] (hereafter MN06) suggest that the response of the MOC to surface buoyancy forcing may be less sensitive to the nature of vertical mixing in a two-hemisphere ocean. We extend earlier numerical work in two major respects. First, MN06 used a zonally averaged model that is based on a severe assumption in the dynamics. In zonally averaged models the zonal pressure difference must be parameterized. MN06 used a simplified closure for the difference, where the Coriolis acceleration is neglected in the equation for the meridional velocity. Thus, in spite of the important insights that this closure has provided in this and earlier work, a model that is more geophysically grounded seems warranted. The present study relies on a model that makes the connection with the ocean circulation perhaps more apparent [*Wright et al*., 1995]. Second, we explore the possibility of self-sustained or self-excited oscillations of the flow under constant freshwater forcing when κ_v depends on vertical stability. Such oscillations have been found in a hierarchy of ocean models—most of which are based on a κ_v that does not depend on vertical stability—and are often suggested as being relevant to the study of the rapid climate changes of the last glacial period (e.g., *Winton and Sarachik* [1993]). *Paul and Schulz* [2002] reported self-excited oscillations in a coupled climate model whose oceanic component is a zonally averaged model based on the closure of *Wright et al*. [1995] and a fixed κ_v. Self-sustained oscillations with a stability-dependent κ_v have been found in a zonally averaged model based on the simplified closure described above [*Olsen et al*., 2005]. Here we examine whether self-excited oscillations occur with a stability-dependent κ_v in a zonally averaged model based on the more elaborate closure of *Wright et al*. [1995].

It is perhaps worth being explicit about the limitations of this work. A major limitation is the zonally averaging of the equations of motion. Although an investigation with a three-dimensional (3D) model would clearly be desirable, the use of a zonally averaged model is motivated by the numerical integrations (long and numerous) that are required to illustrate and understand the dynamical effects of a stability-dependent κ_v. Other limitations of this work are the crude representation of the thermodynamical interactions with the atmosphere, the omission of the winds, and the absence of topography. More generally, none of the assumptions listed above can be defended rigorously. Rather, they are inspired by our desire to understand the dynamical consequences of a stability-dependent κ_v that may occur in more complete models and perhaps also in the real ocean. Thus, the present work should be viewed as an exercise of geophysical fluid dynamics, with no claim of an accurate representation of the MOC in the real ocean (earlier studies with a similar degree of idealization include the considerable work on the non-rotating flow in a vertical plane; see, e.g., *Dijkstra* [2005]; and references therein).

This paper is organized as follows. Section 2 reviews theoretical arguments for the importance of the nature of vertical mixing for the meridional overturning circulation in the ocean. The numerical model used to explore the dynamical effects of a stability-dependent κ_v is described in section 3. These effects are examined for both one-hemisphere (section 4) and two-hemisphere basins (section 5). In section 6 we explore the possibility of time-dependent flows under constant freshwater forcing when κ_v depends on vertical stratification. A summary follows in section 7.

2. THEORETICAL CONSIDERATIONS

2.1. Thermocline Scaling Theory

A formal suggestion of the importance of vertical mixing for the MOC is provided by a scaling theory for the main thermocline (for a short review see, e.g., *Welander* [1986]). Consider a meridional section in a hypothetical ocean where a surface of equal density (isopycnal surface) outcrops at high latitudes (Figure 1). The depth of the isopycnal surface at low latitudes is H, which is referred to below as the 'depth of the thermocline'. Because the surface outcrops, the equator-to-pole density contrast at the surface is equal to the vertical density contrast at low latitudes; both contrasts are thus denoted by the same symbol, $\Delta\rho$ (the effect of compression on density can be neglected for the present argument). The flow is assumed to be in hydrostatic and geostrophic balances. In the Boussinesq approximation these lead to the thermal wind relation,

$$f\frac{\partial v}{\partial z} = -\frac{g}{\rho_0}\frac{\partial \rho}{\partial x}. \tag{2}$$

Here x is the longitude, z is depth, v is the meridional velocity, f is the Coriolis parameter, g is the acceleration due to gravity, and ρ is the density (ρ_0 is a reference value). Thus, a vertical shear in the meridional flow should be associated with a zonal gradient of density. Relation (2) provides a scaling for the meridional transport of volume, Ψ_M,

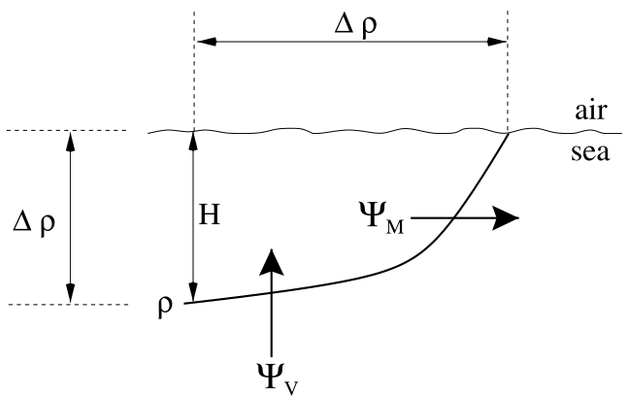

Figure 1. Ocean density field from the low to high latitudes as envisioned by thermocline scaling theory. The depth scale for the thermocline at low latitudes is H. The vertical density difference over H at low latitudes is equal to the horizontal density difference at the surface between the low and high latitudes, as the surfaces of equal density outcrop at high latitudes. According to the theory, the density field is associated with a poleward volume flux at the surface (Ψ_M), which is balanced by a vertical volume flux into the thermocline (Ψ_V).

$$\Psi_M \sim \Delta\rho H^2. \tag{3}$$

Here it was *assumed* that the zonal density difference is proportional to the meridional density difference. A scaling for the transport of volume across the isopycnal surface, Ψ_V, is provided by the assumption of a vertical balance in the density equation,

$$w\frac{\partial \rho}{\partial z} = \kappa_v \frac{\partial^2 \rho}{\partial z^2}, \tag{4}$$

where w is the vertical velocity. This relation yields

$$\Psi_V \sim \frac{A\kappa_v}{H}, \tag{5}$$

where A is the area of the upwelling region. If the poleward flow is entirely balanced by the vertical flow into the thermocline, $\Psi_M = \Psi_V = \Psi$. Two well-known relationships are then obtained,

$$H \sim \Delta\rho^{-1/3}\kappa_v^{1/3}, \tag{6}$$

$$\Psi \sim \Delta\rho^{1/3}\kappa_v^{2/3}. \tag{7}$$

The depth of the thermocline increases and the strength of the flow decreases as the equator-to-pole density contrast is reduced, assuming that the vertical diffusivity is constant. On the other hand, they both increase with the vertical diffusivity. Tests of the scaling laws (6–7) from results with numerical models have had a variable success (e.g., *Wright and Stocker* [1992]; *Park and Bryan* [2001]; *Mohammad and Nilsson* [2004]; *Nilsson et al*. [2003]) and probably deserve a review in their own right.

Consider now a case where κ_v is not constant (e.g., *Nilsson et al*. [2003]). A simple approach, which is based on an argument originally put forward by *Kato and Phillips* [1969], is to postulate that energy must be supplied at a certain rate in order to mix deep dense waters with overlying light waters. This condition is written as

$$E = -g\int \kappa_v \frac{\partial \rho}{\partial z} dz > 0, \tag{8}$$

where E is the rate of energy supply per unit surface area; in the ocean the supply is thought to be met by the rate of work done by the winds and by the dissipation of tidal motions (e.g., *Munk and Wunsch* [1998]; *Wunsch and Ferrari* [2004]). If κ_v is vertically uniform,

$$\kappa_v = \frac{E}{g\Delta\rho}. \tag{9}$$

Thus, in an ocean where the energy supply is fixed, the vertical diffusivity would decrease with increasing bottom-to-top density difference. Inserting (9) into (6–7) gives

$$H \sim \Delta\rho^{-2/3}(AE)^{1/3}, \tag{10}$$

$$\Psi \sim \Delta\rho^{-1/3}(AE)^{2/3}, \tag{11}$$

where AE is the integral of E over the stratified upwelling region of surface area A. Thus, when κ_v depends on vertical stability, the depth of the thermocline increases as the equator-to-pole density contrast is reduced, which is qualitatively similar to the case with fixed κ_v (although the degree of sensitivity is higher than for that case). On the other hand, the strength of the flow increases with decreasing density contrast, which is opposite to the case with fixed κ_v. The fundamental mechanism responsible for the opposite reaction lies in the adjustment of the thermocline depth to a change in the density contrast. The adjustment to, say, a decrease of $\Delta\rho$ is larger if κ_v is stability-dependent ($H \sim \Delta\rho^{-2/3}$) than if it is constant ($H \sim \Delta\rho^{-1/3}$), owing to the extra deepening of the thermocline caused by the enhanced vertical mixing. Because the flow varies with $\Delta\rho$ to the first power and with H to the second power, the effect of thermocline adjustment overcomes the direct effect of a flow reduction caused by the reduced meridional density contrast, so that this flow increases in strength.

The contrasting influences of a fixed κ_v and of a stability-dependent κ_v as predicted by these simple scaling arguments have been tested by simulations with numerical models of buoyancy-driven flows assuming (i) a restoring boundary condition for temperature (surface temperatures relaxed to specified values); (ii) a constant salinity; and (iii) a linear equation of state. In their zonally averaged model for a one-hemisphere basin, *Mohammad and Nilsson* [2004] (hereafter MN04) showed that the equilibrium responses of the thermocline depth and overturning strength to changes in $\Delta\rho$ follow approximately (6–7) when κ_v is fixed and (10–11) when it varies with vertical stability. If the model domain extends over two hemispheres, the domain being symmetric about the equator, the simulated flows exhibit two overturning cells: a strong cell centered in the hemisphere where $\Delta\rho$ is largest (the 'dominant' hemisphere) and a weaker cell in the other hemisphere (the 'subordinate' hemisphere) (MN06). These authors found that the model results still corroborate the scaling laws (6–7) (for fixed κ_v) and (10–11) (for stability-dependent κ_v), if the degree of asymmetry in surface buoyancy forcing between the two hemispheres is maintained (i.e., if the ratio between the pole-to-pole density difference to the equator-to-pole density difference is fixed). Finally, *Nilsson et al*. [2003] used a 3D model based on the primitive equations and confined in a single hemisphere. They found that the thermocline depth and the overturning strength follow approximately (6–7) when κ_v is constant and (10–11) when it is stability-dependent.

Note that other scaling laws for the oceanic thermocline have been developed (e.g., *Samelson and Vallis* [1997]; *Vallis* [2000]). These authors reported a scaling that assumes that the thermocline is composed of two different layers with distinct dynamical regimes: an upper, 'ventilated' thermocline where the motion is adiabatic and a lower, 'internal' thermocline which is diffusive. The upper thermocline comprises fluid advected downward by Ekman pumping in the subtropical gyre, which allows an explicit consideration of the wind in the theory. The thickness of the upper (H_U) and lower thermoclines (H_L) obey

$$H_U \sim \Delta\rho^{-1/2} W_E^{1/2}, \tag{12}$$

$$H_L \sim \Delta\rho^{-1/4} W_E^{-1/4} \kappa_v^{1/2}, \tag{13}$$

where W_E is the imposed Ekman velocity. Below only buoyancy-driven flows are considered and the discussion is restricted to the scaling laws (6–7) (constant κ_v) and (10–11) (stability-dependent κ_v).

2.2. Sensitivity to Freshwater Forcing

Nilsson and Walin [2001] (hereafter NW01) explored the dynamical consequences of a stability-dependent vertical mixing (more exactly, upwelling) in a two-layer model (Figure 1), when the fluid density depends on both temperature and salinity. The distinction between the two density components allowed the fundamental effect of freshwater forcing on the MOC to be investigated [*Stommel*, 1961]. The following assumptions were made regarding the poleward and vertical flows:

$$\Psi_M \sim \Delta\rho H^2, \tag{14}$$

$$\Psi_V \sim \Delta\rho^{-\zeta} H^{-\eta}, \tag{15}$$

where ζ, $\eta \geq 0$. The authors found that when the upwelling does not depend on vertical stability ($\zeta = 0$ and $\eta = 1$) the flow exhibits different equilibria for the same freshwater forcing, consistent with the model of *Stommel* [1961] (Figure 2). On the other hand, when the upwelling depends on stability ($\zeta = \eta = 1$), there is only a single equilibrium for a given forcing and the freshwater forcing *amplifies* the strength of the flow (dashed line in Figure 2). The feedback

between salinity and circulation anomalies, which is positive when the upwelling is stability-independent, becomes negative when it is stability-dependent. Thus, the circulation is stable to any (infnitesimal) perturbations in the forcing.

The theoretical relationships of NW01 have been compared to simulations with numerical models of buoyancy-driven flows under mixed boundary conditions (surface temperature relaxed and surface salinity flux imposed). For a one-hemisphere basin, the strength of the MOC decreases with increasing freshwater forcing if κ_v is constant, whereas it increases with increasing forcing if κ_v is stability-dependent (MN04); these results are qualitatively consistent with the theory (Figure 2). For a two-hemisphere basin, on the other hand, the strength of the MOC increases with increased freshwater forcing (symmetric about the equator) for both representations of vertical mixing if the circulation is equatorially asymmetric (MN06). Thus, the theoretical relationships developed by NW01 may not hold in a two-hemisphere basin.

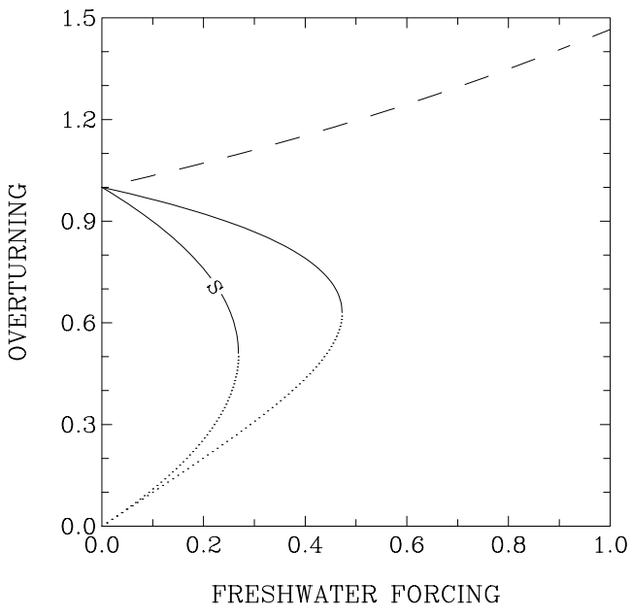

Figure 2. Equilibrium responses of the overturning strength to surface freshwater forcing in the two-layer model of *Nilsson and Walin* [2001]. The actual response depends on the nature of the upwelling into the low latitude thermocline, which is represented as $\Psi_V \sim \Delta\rho^{-\zeta}H^{-\eta}$. If the upwelling is independent on vertical density stratification ($\zeta = 0$ and $\eta = 1$), the overturning strength decreases with freshwater forcing (solid line; the unstable branch is shown by the dotted line). If upwelling depends on vertical density stratification ($\zeta = 1$ and $\eta = 1$), the overturning strength increases with freshwater forcing (dashed line; there is no unstable branch for this case). The solid line labeled with 'S' displays a model that operates similarly to the model of *Stommel* [1961] (the unstable branch for this case is also shown by a dotted line).

3. NUMERICAL MODEL

In this section we describe the zonally averaged model that is used to examine further the theoretical arguments summarized in section 2. Only a brief description is given; details can be found in the references provided below. Two different idealized domains are considered, each being characterized by a flat bottom at a depth $D = 4000$ m, vertical lateral boundaries, and a zonal width (L) equivalent to 70°. A first domain extends from 4°S to 76°N and the second domain extends from 76°S to 76°N. For both domains, the grid has a cell that straddles the equator in order to permit the use of the model employed in this work [*Wright et al*., 1995]. For both domains, the grid has a meridional resolution of 8° and a vertical resolution that is variable with depth: 50 m between 0–300 m, 100 m between 300–1000 m, 125 m between 1000–1500 m, and 250 m below (27 vertical layers).

3.1. Equations of Motion

The following approximations in the equations of motion are made. The fluid is incompressible and Boussinesq, and the flow has a small Rossby number and is in hydrostatic balance. Friction in the equations for horizontal momentum is represented as Fickian diffusion in the zonal direction, which provides the simplest model of dissipation in the western boundary layer. These equations are thus

$$-fv = -\frac{1}{\rho_0}\frac{\partial p}{\partial x} + \frac{\partial}{\partial x}\left(A\frac{\partial u}{\partial x}\right), \tag{16}$$

$$fu = -\frac{1}{\rho_0}\frac{\partial p}{\partial y} + \frac{\partial}{\partial x}\left(A\frac{\partial v}{\partial x}\right). \tag{17}$$

Here x (y) is the longitude (latitude), u (v) is the zonal (meridional) velocity, p is pressure, and A is a viscosity coefficient. Cross-differentiating gives an equation for the relative vorticity, $\zeta = \partial v/\partial x - \partial u/\partial y$:

$$\frac{\partial}{\partial x}(fu) + \frac{\partial}{\partial y}(fv) = \frac{\partial}{\partial x}\left(A\frac{\partial \zeta}{\partial x}\right). \tag{18}$$

Integrating from the western boundary (at x_0) to the eastern boundary gives, with the conditions of no normal flow and no slip at these boundaries,

$$f\frac{\partial}{\partial y}(L\bar{v}) + L\bar{v}\frac{\partial f}{\partial y} = -A\frac{\partial \zeta}{\partial x}\Big|_{x_0}. \tag{19}$$

Here $\bar{v}$ is the zonal average of meridional velocity and the dissipation of relative vorticity at the eastern boundary has been neglected. Thus, the vortex stretching or compression

caused by meridional variations in the meridional flow is balanced by (i) the advection of planetary vorticity and (ii) the dissipation of relative vorticity in the western boundary layer. In 3D models, the dissipation must be properly represented, whereas in zonally averaged models it must be parameterized [*Wright et al*., 1995].

These authors developed a parameterization of the dissipation based on well-defined physical assumptions (see also *Wright et al*. [1998]). Consider the integrated meridional flow $(L\bar{v})$ as the sum of the flows in the western boundary layer with zonal width $\delta\,(\delta\bar{v}^{\delta})$ and in the inviscid interior with zonal width $l\,(l\bar{v}^{l})$. For spherical coordinates, the parameterization of vorticity dissipation leads to the following balances:

$$\frac{\partial}{\partial z}(\delta\bar{v}^{\delta}) = \frac{2g}{f}\left[\gamma_2\left(\frac{f}{f_{\text{end}}}\right)^{\gamma_1}(\bar{\sigma}_{\text{end}} - \bar{\sigma}_{\text{eq}}) + |f|^{\gamma_1}\int_{\phi}^{\phi_{\text{end}}} |f|^{-\gamma_1}\frac{\partial\bar{\sigma}}{\partial\phi'}d\phi'\right], \tag{20}$$

$$\frac{\partial}{\partial z}(l\bar{v}^{l}) = \frac{2g}{f}(\bar{\sigma} - \bar{\sigma}_{\text{eq}}). \tag{21}$$

Here ϕ is latitude, $\bar{\sigma} = (\bar{\rho} - \rho_0)/\rho_0$ is the zonal average of density anomaly, subscript 'end' denotes a value at the northern or southern end of the domain, and subscript 'eq' denotes a value at the equator. The closure scheme includes two parameters: γ_1 and γ_2. The first parameter describes the dissipation of vorticity in the unresolved western boundary layer and the second describes the net overturning in the unresolved high-latitude boundary layers that are embedded in the southernmost and northernmost grid cells of the model. The density anomaly $\bar{\sigma}$ is computed from a linear equation of state,

$$\bar{\sigma} = -\alpha(\bar{T} - T_0) + \beta(\bar{S} - S_0), \tag{22}$$

where $\bar{T}$ $(\bar{S})$ is the zonal average of temperature (salinity), α is the coefficient of thermal expansion, β is the coefficient of haline contraction, and (T_0, S_0) are reference values. The equations for $\bar{T}$ and $\bar{S}$ are (e.g., *Wright and Stocker* [1991]):

$$\frac{\partial\bar{T}}{\partial t} + \frac{\partial}{\partial s}\left(\frac{c\bar{v}}{a}\bar{T}\right) + \frac{\partial}{\partial z}(\bar{w}\bar{T}) = \frac{\partial}{\partial s}\left(\frac{c^2\kappa_h}{a^2}\frac{\partial\bar{T}}{\partial s}\right) + \frac{\partial}{\partial z}\left(\kappa_v\frac{\partial\bar{T}}{\partial z}\right) + q_T, \tag{23}$$

$$\frac{\partial\bar{S}}{\partial t} + \frac{\partial}{\partial s}\left(\frac{c\bar{v}}{a}\bar{S}\right) + \frac{\partial}{\partial z}(\bar{w}\bar{S}) = \frac{\partial}{\partial s}\left(\frac{c^2\kappa_h}{a^2}\frac{\partial\bar{S}}{\partial s}\right) + \frac{\partial}{\partial z}\left(\kappa_v\frac{\partial\bar{S}}{\partial z}\right) + q_S. \tag{24}$$

Here t is time, $\bar{v}$ $(\bar{w})$ is the zonal average of meridional (vertical) velocity, $c \equiv \cos\phi$, $s \equiv \sin\phi$, a is the earth radius, κ_h (κ_v) is the horizontal (vertical) effective diffusivity, and q_T (q_S) represents the effect of convection on temperature (salinity). In practice, the velocity field is obtained from a stream function ψ,

$$\bar{v} = -\frac{1}{c}\frac{\partial\psi}{\partial z}, \tag{25}$$

$$\bar{w} = \frac{1}{a}\frac{\partial\psi}{\partial s}. \tag{26}$$

Details regarding the method of solution and the convection scheme can be found in *Wright and Stocker* [1991] and *Wright and Stocker* [1992]. Note that no attempt is made here to reduce the effects of numerical diffusion. The values of model parameters used in this work are reported in Table 1.

3.2. Initial and Boundary Conditions

The initial conditions of the model are a state of rest ($v = w = 0$) and uniform T, S (overbars for the dynamical variables are omitted henceforth). The model ocean is subject to restoring or mixed boundary conditions at the surface (wind stress is ignored). In the numerical experiments with restoring boundary condition, salinity is not considered ($S = S_0$) and the heat flux at the surface is given by

$$-\kappa_v\frac{\partial T}{\partial z} = \frac{\Delta z}{\tau}(T - T_*). \tag{27}$$

Here $\Delta z = 50$ m is the thickness of the surface grid cell, $\tau = 50$ d is the restoring time scale, and $T_*(\phi)$ is the restoring temperature. In the experiments with mixed boundary conditions, both salinity and temperature affect the density. The surface heat flux is given by (27), whereas the surface salt flux is

$$-\kappa_v\frac{\partial S}{\partial z} = F, \tag{28}$$

where $F(\phi)$ is imposed. The latitudinal distributions $T_*(\phi)$ and $F(\phi)$ used in our numerical integrations represent idealized conditions of the real ocean (sections 4–5).

3.3. Mixing Representations

Two different representations of vertical mixing are considered, one with a constant diffusivity and one with a stability-dependent diffusivity (MN04; MN06):

$$\kappa_v = \kappa_{v0}, \tag{29}$$

$$\kappa_v = \kappa_{v0}\frac{\Delta\rho_0}{\Delta\rho}. \tag{30}$$

Table 1. Parameters of the zonally averaged ocean model.

Symbol	Definition	Value	Units
a	earth radius	6,371	km
f	Coriolis parameter	$f = 2\Omega \sin \phi$	s^{-1}
Ω	angular velocity of earth rotation	7.27×10^{-5}	s^{-1}
g	acceleration of gravity	9.81	$m\ s^{-2}$
ρ_0	reference density	1028	$kg\ m^{-3}$
κ_h	horizontal effective diffusivity	10^3	$m^2\ s^{-1}$
κ_v	vertical effective diffusivity	variable	$m^2\ s^{-1}$
α	coefficient of thermal expansion	2×10^{-4}	$°C^{-1}$
β	coefficient of haline contraction	8×10^{-4}	
T_0	reference temperature	0	°C
S_0	reference salinity	35	
γ_1	closure parameter[a]	1.1	
γ_2	closure parameter[a]	–0.6	

[a]Based on results from a 3D model [*Wright et al*., 1995].

Here $\kappa_{v0} = 10^{-4}\ m^2\ s^{-1}$, $\Delta\rho = \rho_0(-\alpha\Delta T + \beta\Delta S)$ is the difference between the bottom density and the surface density, and $\Delta\rho_0 = -\rho_0\alpha\Delta T_0$ is a reference difference, where $\Delta T_0 = 25°C$. In the experiments where salinity is not considered, $\Delta\rho = -\rho_0\alpha\Delta T$. Thus, when a stability-dependent diffusivity is assumed, κ_v varies with latitude but not with depth. In order to avoid unrealistically large diffusivity when the water column is close to neutral stability, we use $\kappa_v = \min(\kappa_v, 10^{-3}\ m^2\ s^{-1})$.

3.4. Comparison with Theory

For each numerical experiment two quantities, which describe the depth of the thermocline and the strength of the MOC, are diagnosed in order to compare with the scaling laws for fixed and stability-dependent κ_v (equations 6–7 and 10–11) and with the analytical relationships of NW01 (Figure 2). Both quantities are diagnosed at about the middle latitude of the basin for the single-hemisphere experiments and of the northern hemisphere basin for the two-hemisphere experiments. We follow the definitions given by *Nilsson et al*. [2003], which were used by MN04 and MN06. Thus, the thermocline depth H is taken as

$$H = \int_{-D}^{0} \frac{T(z) - T(-D)}{T(0) - T(-D)}\, dz, \tag{31}$$

where $T(0)$ is the temperature at the surface and $T(-D)$ is the temperature at the bottom. The strength of the MOC is taken as the maximum of the stream function from the bottom to the surface,

$$\Psi_{\max} = \max_{z \in [-D,0]} L\psi(z). \tag{32}$$

This strength is reported in units of Sv (1 Sv $\equiv 10^6\ m^3\ s^{-1}$).

Note that the definition of both the thermocline depth and the overturning strength involve some arbitrariness; for example, they can be diagnosed using different formulas and/or at different latitudes (or they could represent averages over some latitude range). This point should be kept in mind, as the degree of (dis)agreement between the model results and the theory may somewhat depend on how both quantities are computed from the model results.

4. STEADY FLOWS IN THE ONE-HEMISPHERE BASIN

The model domain is first restricted to one hemisphere (more precisely, between 4°S–76°N). Numerical experiments with fixed or stability-dependent κ_v and with restoring or mixed boundary conditions are conducted by integrating the model for 5000 years. The absence of a visible trend in the integrated surface flux of heat at the end of the integrations suggests a nearly steady state. It is instructive to first consider a representative example of the flow (obtained with fixed κ_v and with mixed boundary conditions that are detailed below). The circulation is characterized by a single overturning cell, with water sinking at high latitudes and water rising elsewhere (Figure 3a). At high latitudes temperature and salinity are about vertically uniform, whereas a thermocline and a halocline have developed at low latitudes (Figures 3b–3c). Below, we investigate how the representation of vertical mixing affects the response of this flow to changes in surface buoyancy forcing.

4.1. Restoring Boundary Condition

The model is integrated with the surface boundary condition (27), where

$$T_*(\phi) = \frac{\Delta T}{2}\left(1 + \cos\frac{\pi\phi}{\phi_m}\right). \quad (33)$$

Here ΔT is the equator-to-pole temperature difference and $\phi_m = 80°$ is the meridional extent of the basin. A series of experiments with different values of ΔT are performed. Consider first the results obtained with a constant diffusivity κ_v (relation 29). The depth of the thermocline increases as ΔT decreases (solid circles in Figure 4a). The numerical results follow closely the relationship predicted by scaling theory, $H \sim \Delta T^{-1/3}$. Note also the departures from the theoretical relationship, which are the most pronounced for large values of H. Likewise, the strength of the overturning circulation decreases with a reduced ΔT in a manner that is consistent with theory, i.e., $\Psi_{max} \sim \Delta T^{1/3}$ to a good approximation (solid circles in Figure 4b). The agreement with thermocline scaling theory is concordant with earlier results obtained from a zonally averaged model (MN04) and a 3D model [*Nilsson et al*., 2003].

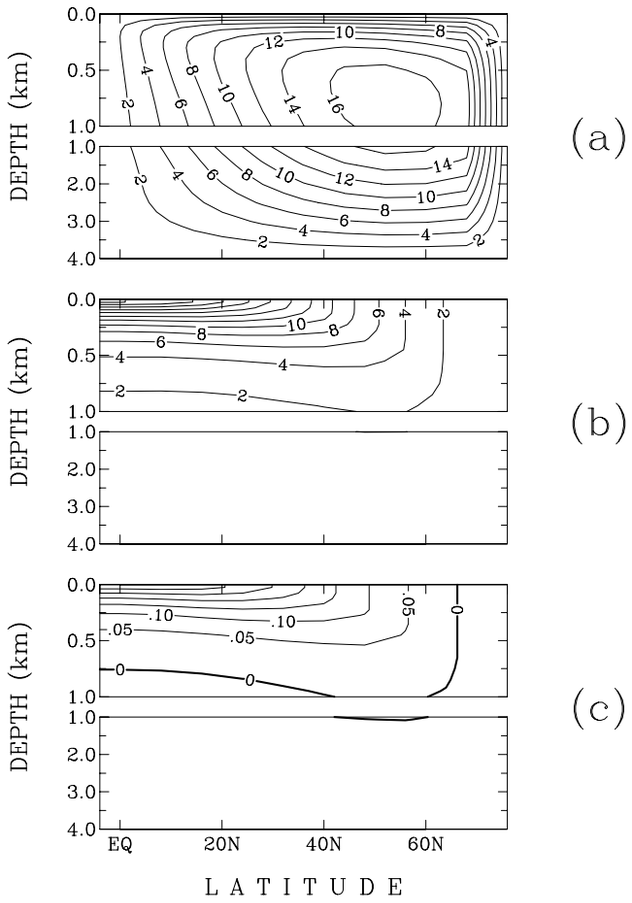

Figure 3. Distribution of (a) the stream function (in Sv), (b) the temperature (°C), and (c) the salinity anomaly (S - S_0) in a single-hemisphere experiment where the flow is subject to mixed boundary conditions and the vertical diffusivity is constant. The contour intervals are 2 Sv, 2°C, and 0.05.

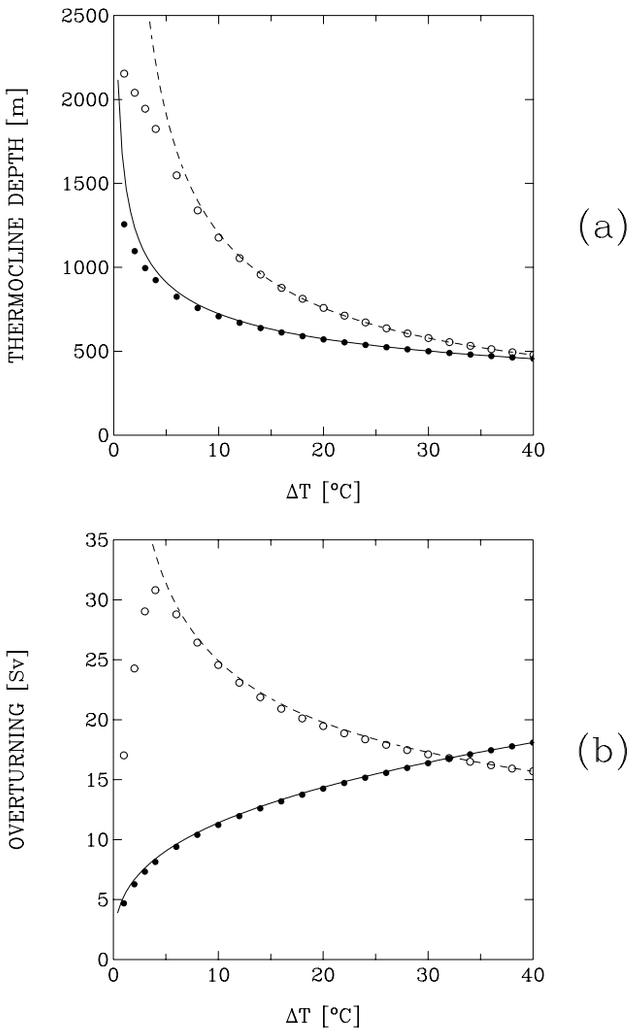

Figure 4. Equilibrium responses of (a) the thermocline depth and (b) the overturning strength to the equator-to-pole temperature difference at the surface in the one-hemisphere model. Results obtained from a fixed κ_v and a stability-dependent κ_v are shown by solid and open circles, respectively. The thermocline depth and overturning strength diagnosed from the model are the values at about the middle latitude of the basin (at 40°N and 36°N, respectively). They are compared to the scaling laws for the oceanic thermocline for the case with fixed κ_v (solid line) and stability-dependent κ_v (dashed). To facilitate the comparison the scaling laws are anchored to the values computed by the numerical model for the largest thermal forcing at the surface ($\Delta T = 40°C$).

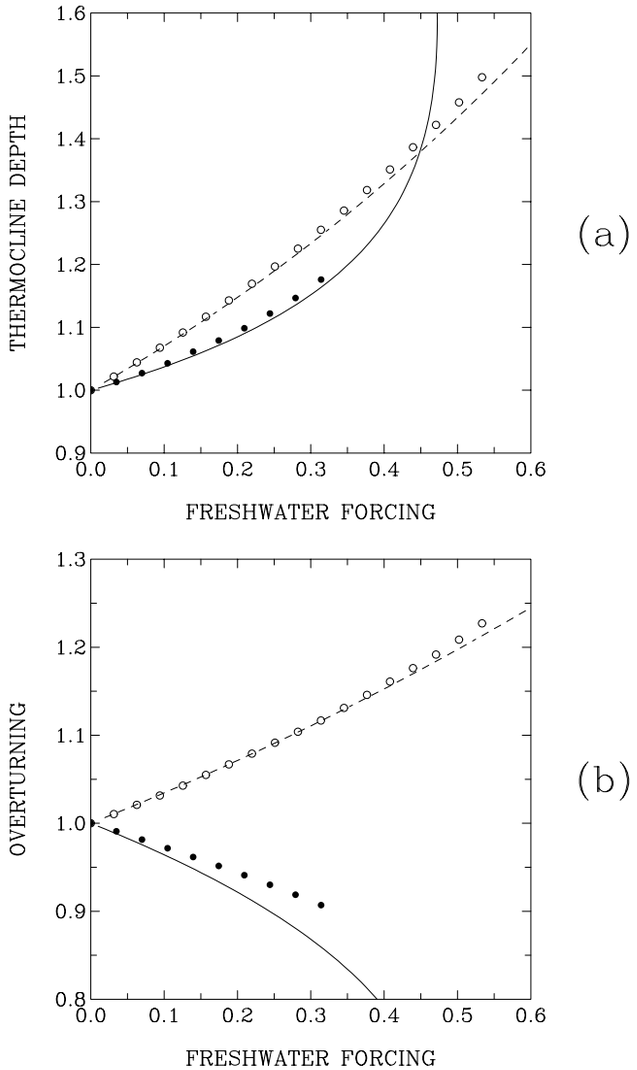

Figure 5. Equilibrium responses of (a) the thermocline depth and (b) the overturning strength to surface freshwater forcing in the one-hemisphere model. Results obtained from a fixed κ_v and a stability-dependent κ_v are shown by solid and open circles, respectively. The thermocline depth and overturning strength diagnosed from the model are the values at about the middle latitude of the basin (at 40°N and 36°N, respectively). Both are normalized to the values simulated by the model for the case where the freshwater forcing vanishes. Likewise, the freshwater forcing is normalized as explained in the text. The model results are compared to the theoretical relationships of *Nilsson and Walin* [2001] for the case with fixed κ_v (solid line) and stability-dependent κ_v (dashed).

Consider then the results obtained with a stability-dependent κ_v (relation 30). Compared to the case with fixed κ_v, the depth of the thermocline increases to a larger extent in response to a reduced ΔT (open circles in Figure 4a). The numerical results are well approximated by the theoretical scaling $H \sim \Delta T^{-2/3}$, except for the experiments characterized by a deep thermocline. In contrast to the case with fixed κ_v, the strength of the overturning increases as ΔT is reduced (open circles in Figure 4b). The agreement with the theoretical scaling is good, i.e., $\Psi_{max} \sim \Delta T^{-1/3}$, except again for the experiments with large H, which show an increase of Ψ_{max} with ΔT. These results also resonate with those obtained in earlier studies (MN04; *Nilsson et al*. [2003]).

Note that the departures of the model from theory in the regime of deep thermocline (Figures 4a–4b) can be rationalized (MN04). In this regime, the depth of the thermocline is not controlled by the vertical advective-diffusive balance of buoyancy but by the basin geometry. Thus, the scaling for the meridional overturning becomes

$$\Psi \sim \Delta\rho D^2. \tag{34}$$

The strength of the MOC varies linearly with the density contrast at the surface and does not depend on the nature of vertical mixing. This provides an explanation for the reversal in the response of the overturning to ΔT as the thermocline becomes very thick (Figure 4b).

4.2. Mixed Boundary Conditions

The model is now integrated with the surface boundary conditions (27–28). Note that in this case the equator-to-pole density contrast ($\Delta\rho$) is not imposed but is partly determined by the dynamics. The distribution of the restoring temperature is given by (33) with $\Delta T = 25$°C. The distribution of the surface salt flux is

$$F(\phi) = -F_0 \cos\frac{\pi\phi}{\phi_m} + F', \tag{35}$$

where F' is a spatially uniform correction allowing the surface integral of F to vanish. In order to permit a comparison with analytical results (NW01) the freshwater forcing at the surface is expressed as a nondimensional quantity (R), which corresponds hereafter to our definition of freshwater forcing (e.g., Figure 5 and Figure 9 later). Let us define first a reference state of the model, where the forcing vanishes ($F(\phi) = 0$). The nondimensional quantity R then corresponds to the ratio between the surface buoyancy forcing associated with the surface salt flux and the thermal buoyancy flux associated with the simulated poleward heat transport in the reference state (e.g., MN04):

$$R = \frac{\beta\langle F\rangle\rho_0 C_p}{\alpha Q_r}. \tag{36}$$

Here $\langle F\rangle$ is the surface integral of $F(\phi)$ over the region where $F(\phi) > 0$ (or ≤ 0), $C_p = 3900$ J kg^{-1} °C^{-1} is the specific heat

capacity of seawater at constant pressure, and Q_r is the depth-integrated heat flux at about the middle latitude of the basin (36°N) in the reference state. In the reference experiment with fixed κ_v, $Q_r = 0.77$ PW, whereas in the reference experiment with a stability-dependent κ_v, $Q_r = 0.86$ PW. Likewise, in order to compare the model results with theory, the values of thermocline depth and overturning strength simulated by the model are normalized to the values of the reference experiments.

Consider first the case with fixed κ_v. The depth of the thermocline increases with the freshwater forcing, the increase being consistent with the theoretical result of NW01 (Figure 5a). Similarly, the strength of the meridional overturning decreases with increasing freshwater forcing in a manner that is consistent with theory, although the agreement is perhaps less apparent (Figure 5b). Note that the model solutions become time-dependent for $R > 0.31$; these solutions, which are not shown in Figure 5, will be examined in section 6.

Consider then the case with a stability-dependent κ_v. Both the thermocline depth and the overturning strength increase with the freshwater forcing, the trends being concordant with the theoretical predictions of NW01 (Figures 5a–5b). Thus, the stability-dependence of the diffusivity leads to an amplification of the MOC as the freshwater forcing intensifies, which is contrary to model results with constant diffusivity obtained here and in earlier studies. Note that solutions become again time-dependent for large values of the forcing, i.e., for $R > 0.53$ (not shown here; section 6).

In summary, our results obtained with the restoring boundary condition agree with those obtained from a zonally averaged model (MN04) and a 3D model (*Nilsson et al*., 2003), in the sense that they can be rationalized by scaling arguments. The results obtained with mixed boundary conditions are also consistent with those of MN04, in the sense that the responses to freshwater forcing follow the predictions from a simple two-layer theory (NW01).

5. STEADY FLOWS IN THE TWO-HEMISPHERE BASIN

The model domain is now extended to include the southern hemisphere (the domain is between 76°S–76°N). It is unclear whether agreement with the scaling laws and the two-layer theory will be found for that case, as the volume exchange at the equator may interfere with the relationships between the thermocline depth, overturning strength, and surface buoyancy forcing in a given hemisphere. Again, a series of numerical experiments with fixed or stability-dependent κ_v and with restoring or mixed boundary conditions is obtained by integrating the model for 5000 years. The absence of a visible trend in the integrated surface flux of heat at the end of the integrations is interpreted as a quasi-steady state.

It is instructive to first examine a representative experiment (obtained with fixed κ_v and with mixed boundary conditions to be described). The flow shows a strong overturning cell centered in the northern (dominant) hemisphere and occupying most of the basin; a weaker cell is confined to the southern (subordinate) hemisphere (Figure 6a). The temperature and salinity distributions are also strongly asymmetric, i.e., the northern hemisphere is colder and saltier than the southern hemisphere and is less vertically stratified (Figures 6b–6c). Below, we explore to which extent the response of this flow to perturbations in surface buoyancy forcing is influenced by the representation of vertical mixing.

5.1. Restoring Boundary Condition

The model is again integrated with the surface boundary condition (27) and with salinity omitted ($S = S_0$). The distribution of the restoring temperature is (MN06)

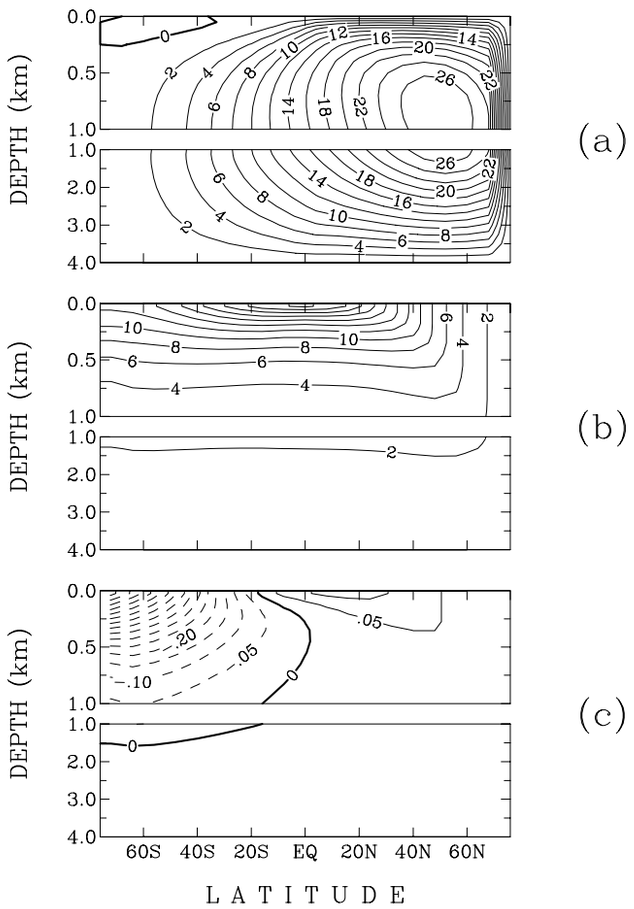

Figure 6. Distribution of (a) the stream function (in Sv), (b) the temperature (°C), and (c) the salinity anomaly ($S - S_0$) in a two-hemisphere experiment where the flow is subject to mixed boundary conditions and the vertical diffusivity is constant. The contour intervals are 2 Sv, 2°C, and 0.05.

$$T_*(\phi) = \frac{\Delta T}{2}\left(2\mu + (1-\mu)\left(1+\cos\frac{\pi\phi}{\phi_m}\right)\right) \quad \text{for } \phi \le 0, \quad (37)$$

$$T_*(\phi) = \frac{\Delta T}{2}\left(1+\cos\frac{\pi\phi}{\phi_m}\right) \quad \text{for } \phi > 0. \quad (38)$$

Here $2\phi_m = 152°$ is the meridional extent of the basin and μ is the ratio between the pole-to-pole temperature difference and the equator-to-pole temperature difference in the northern hemisphere. For $\mu = 0$, the restoring temperature is symmetric about the equator, whereas for $\mu = 1$ the restoring temperature is constant throughout the southern hemisphere, the distribution $T_*(\phi)$ being unchanged in the northern hemisphere. Thus, μ is a measure of the degree of interhemispheric asymmetry in the thermal (or buoyancy) forcing.

Consider first a series of experiments with $\mu = 0.5$ and different values of the equator-to-pole temperature contrast in the northern hemisphere (ΔT). Thus, the degree of asymmetry in thermal forcing is identical among the experiments. The responses of the thermocline depth and of the overturning strength to varying ΔT (Figures 7a–7b) are qualitatively similar to those simulated for a single-hemisphere basin (Figures 4a–4b). They remain consistent with the responses predicted from scaling theory, i.e., $H \sim \Delta T^{-1/3}$ and $\Psi_{max} \sim \Delta T^{1/3}$ when the diffusivity is fixed and $H \sim \Delta T^{-2/3}$ and $\Psi_{max} \sim \Delta T^{-1/3}$ when it varies with vertical stratification. Note that the degree of agreement with theory varies with μ; for example, a set of experiments conducted with $\mu = 0.1$ shows that Ψ_{max} still increases monotonically with decreasing ΔT but in a way that is different from that envisioned by theory (not shown). Again, large departures between the model results and the scaling laws occur as the thermocline becomes very deep (Figures 7a–7b). Thus, the existence of a volume exchange at the equator does not alter the dependencies of the MOC on the thermal forcing: the strength of the overturning in the dominant hemisphere remains controlled by the thermal forcing in that hemisphere. MN06 obtained similar results with a different zonally averaged model.

Consider then the case where the degree of asymmetry in thermal forcing is varied, keeping ΔT unchanged ($\Delta T = 25°C$). The thermocline depth and overturning strength in the northern hemisphere exhibit relatively large increases in response to increased asymmetry for small values of μ and relatively small variations for large values of μ (Figures 8a–8b). *Klinger and Marotzke* [1999] reported a similar result from experiments with a 3D model based on the primitive equations, i.e., the MOC in the dominant hemisphere shows a large increase when the forcing from symmetric becomes asymmetric. The representation of vertical mixing has a relatively small influence (Figures 8a–8b): if κ_v is fixed both H and Ψ_{max} show small increases over most of the μ-range, whereas if κ_v depends on vertical stability they exhibit small decreases. Thus, the dynamical effects of the nature of vertical mixing depends on the nature of the perturbation in surface buoyancy forcing: if the forcing varies in a way that

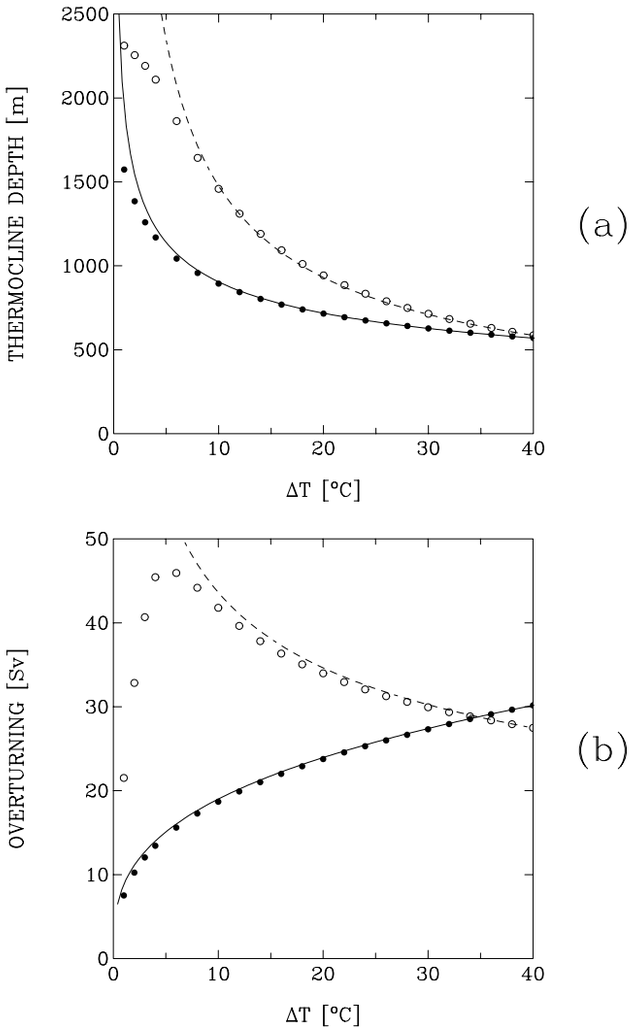

Figure 7. Equilibrium responses of (a) the thermocline depth and (b) the overturning strength to the equator-to-pole temperature difference at the surface in the two-hemisphere model. Results obtained from a fixed κ_v and a stability-dependent κ are shown by solid and open circles, respectively. The thermocline depth and overturning strength diagnosed from the model are the values at about the middle latitude in the northern hemisphere (at 40°N and 36°N, respectively). They are compared to the scaling laws for the oceanic thermocline for the case with fixed κ_v (solid line) and stability-dependent κ_v (dashed). To facilitate the comparison the scaling laws are anchored to the values computed by the numerical model for the largest thermal forcing at the surface ($\Delta T = 40°C$).

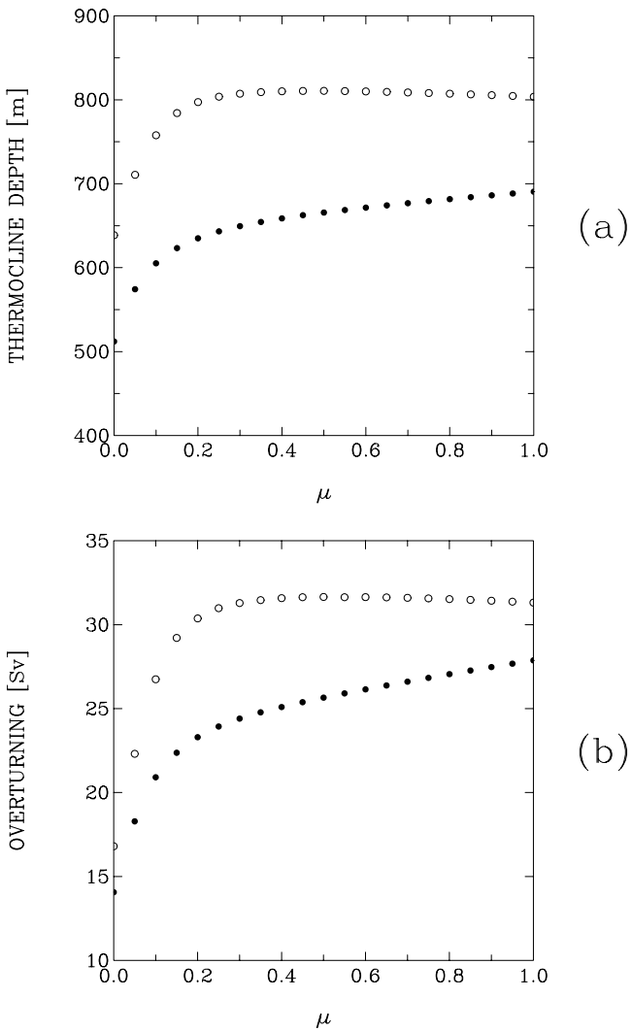

Figure 8. Equilibrium responses of (a) the thermocline depth and (b) the overturning strength to the degree of interhemispheric asymmetry in buoyancy (thermal) forcing. Results obtained from a fixed κ_v and a stability-dependent κ_v are shown by solid and open circles, respectively. The thermocline depth and overturning strength are the values at about the middle latitude in the northern hemisphere (at 40°N and 36°N, respectively).

preserves the asymmetry between the two hemispheres, these effects are important, whereas if the asymmetry is altered, these effects are relatively minor. This finding resonates with the result obtained by MN06.

It is perhaps noteworthy, however, that the overturning strength in the dominant hemisphere is generally less sensitive to the degree of asymmetry in thermal forcing when the diffusivity depends on vertical stability (Figure 8b). In this case, the responses of the thermocline depth and overturning strength saturate already for $\mu \sim 0.3$ (Figures 8a–8b). For constant κ_v, on the other hand, both quantities vary more gradually with μ.

5.2. Mixed Boundary Conditions

We now integrate the model with the restoring temperature (37–38) (with $\Delta T = 25$°C and $\mu = 0.5$) and the flux condition (35) (with $\phi_m = 76°$ now corresponding to half the meridional extent of the basin). Thus, the thermal forcing is not symmetric about the equator, whereas the haline forcing is—the salt flux being into the ocean near the equator and out of the ocean at high latitudes. The surface salt flux, the depth of the thermocline, and the strength of the overturning circulation are all normalized so as to permit a comparison with the theoretical relationships of NW01. Thus, it is assumed that the symmetric freshwater forcing (35) is an appropriate form to compare against theory. For fixed κ_v, the poleward heat flux at 36°N of the reference experiment (Q_r) amounts to 0.87 PW. For a stability-dependent κ_v, Q_r reaches 1.0 PW.

For both representations of vertical mixing, the thermocline depth and overturning strength increase with freshwater forcing (Figures 9a–9b). In contrast to the experiments for a one-hemisphere basin, the model results show strong departures from the theoretical relationships of NW01. Thus, the theory does not adequately represent the sensitivity of the MOC to freshwater forcing in the two-hemisphere model. These results are in conformity with those obtained by MN06 when the circulation is asymmetric about the equator.

The sensitivity of the overturning strength to freshwater forcing (Figure 9b) is interpreted as follows. When the circulation is asymmetric the surface freshwater flux, albeit symmetric, tends to create an asymmetric salinity field that reinforces the equatorial density asymmetry due to the temperature field. The reason is that the equator-to-pole salinity difference is more sensitive to the freshwater forcing in the subordinate hemisphere, where the circulation is weaker than in the dominant hemisphere. Hence, enhancing the freshwater forcing increases also the pole-to-pole density difference.

Two further comments regarding the dynamical responses of the two-hemisphere model to freshwater forcing are in order. First, in contrast to earlier work (MN06), the symmetric circulation about the equator simulated with our model (with $\mu = 0$, not shown) does not exhibit a spontaneous transition to an asymmetric circulation for large freshwater forcing; for large freshwater forcing the circulation remains symmetric but the overturning cell of each hemisphere becomes reversed (water sinking near the equator and water rising elsewhere). For this reason, only the responses of the asymmetric circulation to the forcing have been investigated here. Second, the asymmetric flow exhibits a dramatic change for large freshwater forcing ($R > 0.23$) when κ_v is

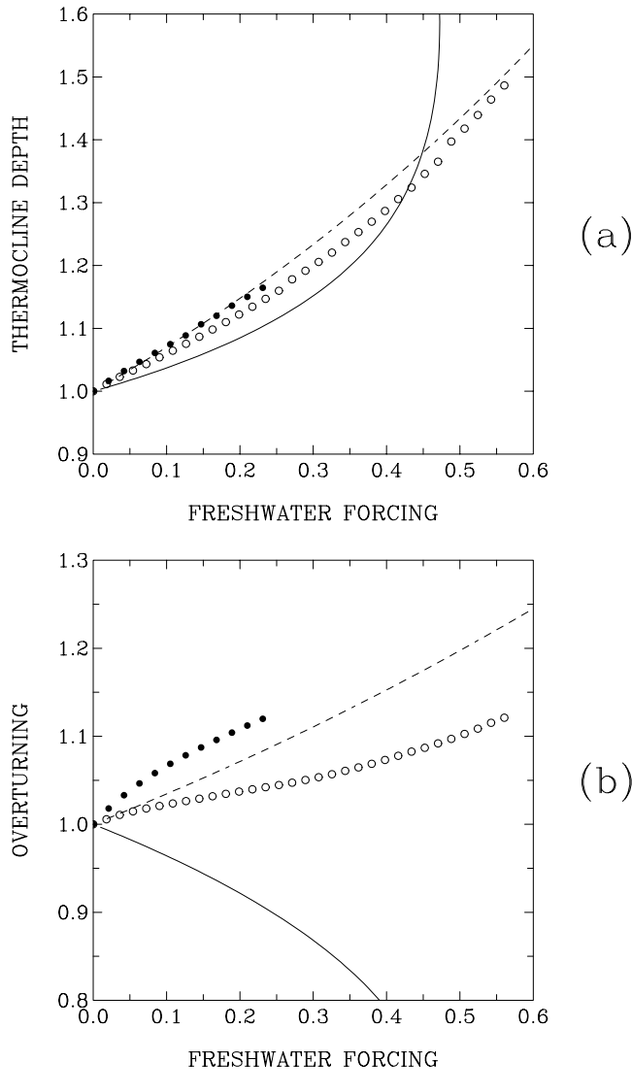

Figure 9. Equilibrium responses of (a) the thermocline depth and (b) the overturning strength to surface freshwater forcing in the two-hemisphere model. Results obtained from a fixed κ_v and with a stability-dependent κ_v are shown by solid and open circles, respectively. The thermocline depth and overturning strength diagnosed from the model are the values at about the middle latitude in the northern hemisphere (at 40°N and 36°N, respectively). Both are normalized to the values simulated by the model for the case where the freshwater forcing vanishes. Likewise, the freshwater forcing is normalized as explained in the text. The model results are compared to the theoretical relationships of *Nilsson and Walin* (2001) for the case with fixed κ_v (solid line) and stability-dependent κ_v (dashed).

constant; the resulting flow is stable and almost symmetric about the equator with, again, water sinking near the equator and water rising elsewhere (these solutions are not shown in Figures 9a–9b). On the other hand, time-dependent solutions are found for large freshwater forcing (for $R > 0.56$) when κ_v varies with vertical stability. A description of the time-dependent solutions obtained for the single-hemisphere basin and the two-hemisphere basin is provided in the next section.

6. UNSTEADY FLOWS

In this section, we examine numerical experiments that are characterized by a variable flow under mixed boundary conditions. Time-dependent solutions are obtained for a single-hemisphere basin when κ_v is either constant or stability-dependent and for a two-hemisphere basin when κ_v is stability-dependent. In the absence of a theoretical framework for the time-dependence, the discussion below is mostly descriptive.

6.1. One-Hemisphere Basin

Consider as an example the time-dependent solution obtained with fixed κ_v and $R = 0.35$ (Figures 10a–10b). Both the thermocline depth at the equator and the maximum overturning strength in the basin exhibit quasi-periodic variations. Initially, the thermocline is relatively shallow and the overturning is in the 'direct' mode with the equator-to-pole density difference dominated by the temperature difference. This flow is destabilized at the surface by the net supply of salt at low latitudes and the net removal of salt at high latitudes. Eventually, salinity dominates temperature in the meridional density difference, leading to a new state with a deeper equatorial thermocline and a reverse overturning with water sinking at the equator and water upwelling elsewhere. This reverse flow, however, is also unstable as the warm water that sinks near the equator is transported poleward below colder water, which decreases the static stability of the water column at high latitudes. Eventually, convection sets it and the reverse flow is interrupted by a violent, direct overturning of several hundreds of Sv (a *flush*), reported previously for zonally averaged and 3D models (e.g., *Marotzke* [1989]; *Wright and Stocker* [1991]). After the flush, the surface temperatures are quickly restored and the surface salinities evolve again towards positive anomalies near the equator and negative anomalies at high latitudes under the effect of surface salt fluxes. This state becomes ultimately destabilized and the cycle repeats itself. Note that for even larger freshwater forcing (e.g., $R = 0.70$), the flow does not display quasi-periodic variations but stays in the reverse mode dominated by salinity differences (not shown).

Time-dependence of the flow occurs for larger freshwater forcing if κ_v depends on vertical stability (Figure 5). Consider the experiment obtained with $R = 0.56$ (thick lines in Figure 11). The overturning strength exhibits a time evolution that is qualitatively similar to the one simulated with fixed κ_v (Figure 10b); quantitative differences between the

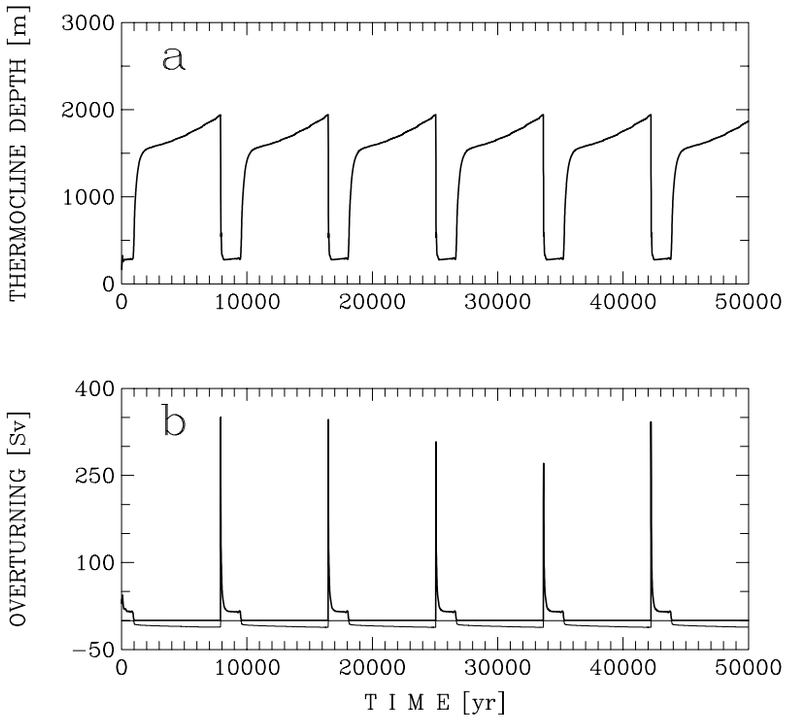

Figure 10. Time evolution of (a) the thermocline depth at the equator and (b) the overturning strength in a single-hemisphere experiment with constant κ_v and $R = 0.35$. In panel (b) both the minimum and maximum values of the stream function in the basin are shown (thin and thick lines, respectively).

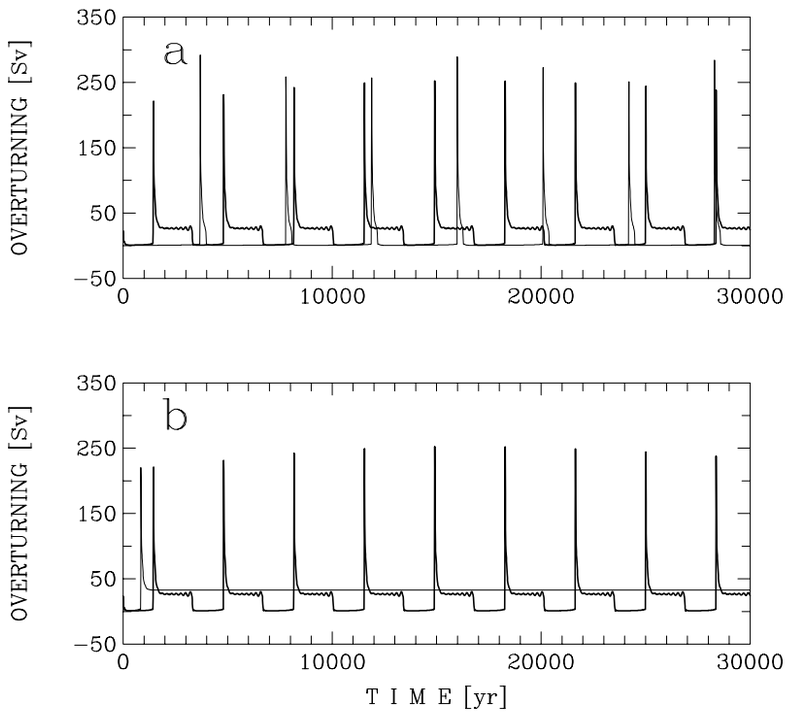

Figure 11. Time evolution of the maximum stream function in different single-hemisphere experiments with a stability-dependent κ_v and R = 0.56. (a) Experiments with a mixing energy of 5.0 mW m^{-2} (thick line) and 5.0 × 0.5 mW m^{-2} (thin line). (b) Experiments with a mixing energy of 5.0 mW m^{-2} (thick line) and 5.0 × 1.5 mW m^{-2} (thin line).

two solutions are due to differences in freshwater forcing as well as in mixing representation. It is instructive to assess the influence of the mixing energy E on the time evolution of the flow. For the experiment described above, $E = g\kappa_{v0}\Delta\rho_0 = 5.0$ mW m^{-2}. We conduct two other experiments with the same freshwater forcing ($R = 0.56$) but with E reduced or increased by 50%. The lower energy level increases the time intervals during which the flow is reversed and decreases the time intervals during which the flow is in the direct mode (compare thin line with thick line in Figure 11a). In contrast, the higher energy level leads to a direct flow that becomes stable after about one millennium (compare thin line with thick line in Figure 11b). Thus, the energy available for vertical mixing has an important influence on the dynamical response of the flow to large freshwater forcing.

6.2. Two-Hemisphere Basin

We finally examine time-dependent flows obtained under constant freshwater forcing for the two-hemisphere basin. As mentioned above, time-dependent solutions for the two-hemisphere basin are not found if κ_v is fixed: in this case the flow for large amplitude of freshwater forcing evolves into a stable state that is almost symmetric about the equator. Of course, the fact that no time-dependent solutions are found for a two-hemisphere basin with fixed κ_v does not imply that no such solutions exist; they may well occur, for example, for different sets of model parameters that have not been explored here.

Consider as an example the experiment obtained with $R = 0.63$ (using a stability-dependent κ_v) (Figures 12a–12b). The flow presents quasi-periodic variations, as for the single-hemisphere basin. It alternates between a phase of asymmetric circulation, with a shallow thermocline depth at the equator and a strong overturning centered in the northern hemisphere, and a phase of quasi-symmetric circulation, with a deeper equatorial thermocline. Thus, during the second phase, both the thermocline depth at the equator and the overturning strength in the southern hemisphere increase gradually. The warm waters that sink near the equator are transported to high latitudes below colder waters in each hemisphere. Again, this destabilizes the flow and leads eventually to a flush. During the flushes, the maximum stream function in both hemispheres increase rapidly (Figure 12b). As for the single-hemisphere basin, it is instructive to explore the influence of varying levels of mixing

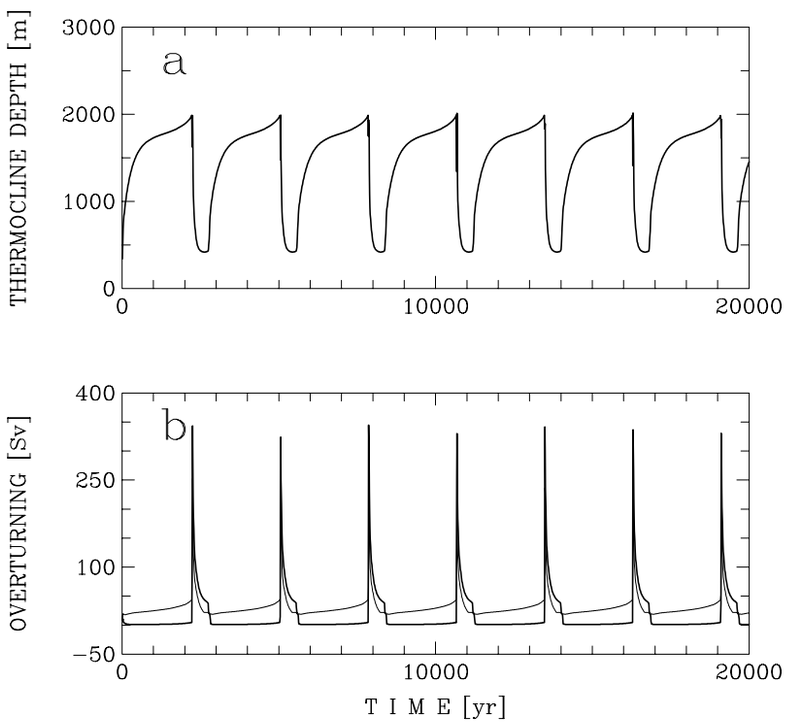

Figure 12. Time evolution of (a) the thermocline depth at the equator and (b) the overturning strength in a two-hemisphere experiment with a stability-dependent κ_v and $R = 0.63$. In panel (b) the maximum values of the stream function in the southern and northern hemispheres are shown (thin and thick lines, respectively).

energy (Figures 13a–13b). The period of the flow oscillations increases when E is reduced and the flow stays stable and asymmetric when E is increased. Thus, the mixing energy has the same qualitative influences on the flow response to large freshwater forcing as in the one-hemisphere basin.

In summary, theoretical considerations for the steady state indicate that the direct flow is stable to any (infinitesimal) perturbation in freshwater forcing if κ_v varies with vertical stability (Figure 2; NW01). The numerical experiments presented here indicate that the direct flow can be destabilized if the forcing is finite in both single- and two-hemisphere basins, leading to quasi-periodic variations. The flow variations have a period that varies with the energy available for vertical mixing. Such variations are absent if the energy level is high enough, the flow then becoming stable and direct in the northern hemisphere.

6.3. Periodicity of the Flow Oscillations

A series of long integrations (50,000 years) allows us to determine with more detail the relationship between the period of flow oscillation and the energy available for vertical mixing for both the one-hemisphere basin and the two-hemisphere basin (Figure 14). At relatively low energy levels, the period decreases gradually with increased mixing energy, the period variations being qualitatively similar for both basins. At high energy levels, the period of flow oscillation rises sharply with increased mixing energy. For very large levels the flow oscillations vanish, as noted earlier.

The variations of the period of flow oscillation with mixing energy could partly be understood from an analogy with the self-sustained or self-excited oscillations that characterize a variety of mechanical and electrical systems. A canonical example of self-sustained system with one degree of freedom is governed by a special form of the van der Pol equation (e.g., *Stoker* [1950]):

$$\ddot{x} + \varepsilon F(\dot{x}) + x = 0, \tag{39}$$

where the dots indicate time differentiation, x is a measure of the departure of the system from rest, ε is a positive constant, and the function $F(\dot{x})$ is given by

$$F(\dot{x}) = -\dot{x} + \frac{\dot{x}^3}{3}. \tag{40}$$

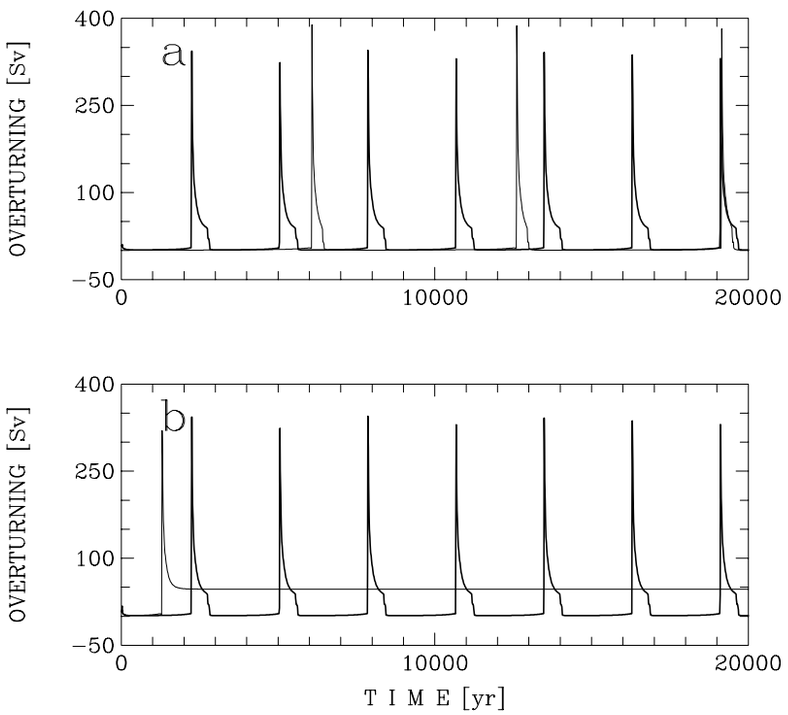

Figure 13. Time evolution of the maximum stream function in the northern hemisphere in different two-hemisphere experiments with a stability-dependent κ_v and $R = 0.63$. (a) Experiments with a mixing energy of 5.0 mW m^{-2} (thick line) and 5.0 × 0.5 mW m^{-2} (thin line). (b) Experiments with a mixing energy of 5.0 mW m^{-2} (thick line) and 5.0 × 1.5 mW m^{-2} (thin line).

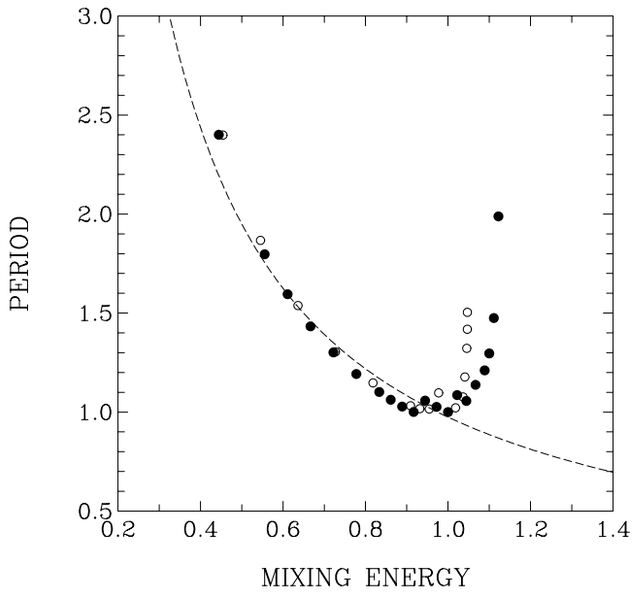

Figure 14. Period of flow oscillation versus the energy available for vertical mixing in the one-hemisphere basin (solid circles) and the two-hemisphere basin (open circles). The period of flow oscillation is taken as the average of the time intervals between subsequent times at which the maximum stream function exceeds 100 Sv. The mixing energies and oscillation periods are normalized to the values obtained for the experiment characterized by a minimum period of flow oscillation for each basin. The model results are compared to a scaling suggested by an analogy of the model behavior with the relaxation oscillations of van der Pol. This scaling law (dashed line) is anchored in the figure so as to maximize the appearance of an agreement of model results with theory.

The damping force $-\varepsilon F(\dot{x})$ tends to increase the amplitude of the departure for small velocities and to decrease it for large velocities. Consequently, a state of rest is not a stable state and an oscillation will be built up from rest even in the absence of external forces. After the transients die out, the system (39–40) is expected to lead to a limit cycle in the phase plane.

Analysis provides some insight into the dynamics of the system (39–40) in the strongly nonlinear limit $\varepsilon \gg 1$ [*Stoker*, 1950]. Introducing two new variables, $\xi \equiv x/\varepsilon$ and $v \equiv \dot{x}$, the motion must satisfy the equation

$$\frac{dv}{d\xi} = \varepsilon^2 \frac{-F(v)-\xi}{v}. \tag{41}$$

In the limit $\varepsilon \gg 1$ different portions can be distinguished in the phase plane (v versus ξ): ones for which $\xi = -F(v) = v - v^3/3$, so that $dv/d\xi = 0$, and others for which $\xi \neq -F(v)$, so that $|dv/d\xi| \gg 1$ or $\xi \approx$ constant. Thus, the motion is relatively slow along the two portions where it occurs along the characteristic curve $\xi = -F(v)$ and is very fast along the two portions where it does not occur along this curve. The period of the oscillations is therefore given by

$$\mathcal{T} = \varepsilon \oint \frac{d\xi}{v} \approx 2\varepsilon \int_{p_1}^{p_2} \frac{d(v - v^3/3)}{v} = 2\varepsilon \left(\ln v - \frac{v^2}{2} \right) \Bigg|_{p_1}^{p_2} \propto \varepsilon, \tag{42}$$

where p_1, p_2 are two positions in the phase plane at the extremities of a portion where $\xi = -F(v) = v - v^3/3$. Thus, jerky oscillations are expected to occur in the limit $\varepsilon \gg 1$, with a period that scales approximately with ε. The different portions of the motion in the phase plane correspond to two major phases that are physically distinct: one during which energy is stored up slowly (in a spring or capacitor) and another in which the energy is discharged rapidly when a certain critical threshold is attained [*Stoker*, 1950].

We hypothesize that the 'relaxation oscillations' of the van der Pol system (39–40) in the limit $\varepsilon \gg 1$ are an analogue of the time-dependent solutions of the numerical model, where the 'energy' is the potential energy stored in the deep ocean. When the flow is reversed (in the one-hemisphere basin) or quasi-symmetric (in the two-hemisphere basin), heat accumulates in the stratified interior, leading to a storage of potential energy. When the vertical salinity stratification cannot stabilize the vertical temperature stratification at high latitudes, a threshold is reached and the potential energy stored in the deep ocean is suddenly released into kinetic energy (the flushes).

In order to assess our hypothesis we determine a plausible analogue of ε in the numerical model and examine whether the relationship between the modeled flow periods and this analogue is consistent with the scaling $\mathcal{T} \sim \varepsilon$ (equation 42). This analogue must have three properties: it must increase monotonically with increased nonlinearity in the dynamics, it must incorporate the mixing energy E, and it must be dimensionless. In the case of a stability-dependent κ_v, the dynamical equations have two sources of nonlinearity: the advection of buoyancy and the vertical mixing of buoyancy (vertical mixing terms in (23–24) are nonlinear as they are proportional to $(\Delta\rho)^{-1}\ \partial^2 T/\partial z^2$ and $(\Delta\rho)^{-1}\ \partial^2 S/\partial z^2$, where $\Delta\rho$ is the bottom-to-top difference of density). Assuming that advection is the dominant source (in the case of fixed κ_v it is the only source of nonlinearity), an analogue of ε would be the ratio of the advection to the vertical mixing of buoyancy. In (23–24) horizontal advection scales as vertical advection owing to the incompressibility of the zonally averaged flow that is implicit in (25–26). Thus, use of the horizontal or vertical advection in the expression for the analogue is immaterial and the advection term in this expression has the general

form $\mathbf{u} \cdot \nabla\rho$. Introducing a characteristic amplitude for, say, the horizontal velocity (U) and characteric length scales for the horizontal (L) and vertical variations of the dynamical fields (H), an analogue of ε would be

$$\mathrm{O}\left(\frac{\mathbf{u}\cdot\nabla\rho}{\kappa_v\partial^2\rho/\partial z^2}\right) = \frac{RoBu\delta}{En}. \tag{43}$$

Here Ro is the Rossby number, Bu is the Burger number, δ is the aspect ratio, and En is a dimensionless mixing energy, i.e.,

$$Ro = \frac{U}{2\Omega L},\ Bu = g\frac{\Delta\rho}{\rho}\frac{H}{(2\Omega L)^2},\ \delta = \frac{H}{L},\ En = \frac{E}{\rho(2\Omega L)^3}. \tag{44}$$

Thus, at any given time, the relative importance of nonlinearity would scale as E^{-1}, i.e., E^{-1} in the numerical model would play the role of ε in the van der Pol equation.

We compare therefore the periods of flow oscillation simulated by the model with the following scaling (dashed line in Figure 14),

$$\mathcal{T} \sim E^{-1}. \tag{45}$$

The modeled periods at small levels of mixing energy follow approximately this scaling, whereas the modeled periods at high levels remain unexplained. Although the comparison is by no means conclusive (the scaling law (45) is intentionally anchored in Figure 14 so as the maximize the appearance of an agreement of the model results with the theoretical scaling), it does suggest that the time-dependent solutions of the numerical model could be fundamentally understood in terms of the van der Pol system (39–40).

7. SUMMARY

A zonally averaged ocean model is used in order to explore the consequences for the meridional overturning circulation of different natures of vertical mixing. In particular, we consider how amplitude changes in the large-scale pattern of freshwater forcing—with net freshwater loss (gain) at low (high) latitudes—affect the MOC. For a single-hemisphere basin, we find that the equilibrium response of the MOC to an increased amplitude of freshwater forcing is a decrease in strength when κ_v is fixed and an increase in strength when it is stability-dependent. On the other hand, for a two-hemisphere basin and an asymmetric MOC about the equator, increased freshwater forcing boosts the overturning in the dominant hemisphere for both representations of vertical mixing (note, however, that a local enhancement of freshwater supply to the sinking regions in the dominant hemisphere would tend to curtail the MOC—at least for the case of a fixed κ_v—as illustrated in numerous studies that focused on the Atlantic). These results resonate with those obtained in earlier studies based on models whose connection with the ocean circulation is perhaps less apparent (NW01; MN04; MN06).

For large but constant freshwater forcing, time-dependent solutions are found for both the single-hemisphere basin and the two-hemisphere basin. These solutions correspond to self-sustained oscillations of the flow and are quasi-periodic (e.g., millennial). The critical forcing beyond which time-dependence occurs is larger when κ_v depends on vertical stability, i.e., the model ocean with fixed mixing energy is more stable to freshwater forcing than the model ocean with fixed diffusivity. For a single-hemisphere basin, time-dependent solutions are found for both fixed and stability-dependent κ_v, whereas for a two-hemisphere basin they occur only when κ_v varies with stratification. The mixing energy affects the response of the flow to freshwater forcing. In particular, the period of the flow oscillations varies with the energy level in a way that can be understood from an analogy with the van der Pol oscillator. Thus, a range of time evolutions of the flow under large freshwater forcing is possible, depending on the nature of vertical mixing and on the amount of energy available.

To apply our results to the real ocean would require a leap that we do not attempt, given the highly idealized character of the model and of the numerical experiments. In our two-basin experiments, the upwelling required to balance sinking in the northern (dominant) hemisphere occurs to a large extent at the mid- and low latitudes with a relatively small contribution at high southern latitudes. The dynamical effects of vertical mixing may be altered if the upwelling in the real ocean takes place mostly at these latitudes. *Toggweiler and Samuels* [1998] used simulations from a 3D model to argue that a MOC powered by winds in the Southern Ocean—the so-called Drake Passage effect—may exist with very little vertical mixing and deep upwelling at low latitudes. *Saenko and Weaver* [2003] used the conceptual model of *Gnanadesikan* [1999] to examine how the nature of vertical mixing affects the MOC in the presence of a circumpolar 'Southern Ocean'. In this model, upwelling occurs in the low latitudes as well as in the Southern Ocean where the net upwelling is the difference between northward Ekman transport and southward eddy transport across the circumpolar current. Analysis shows that the equilibrium response of the MOC to changes in the equator-to-pole density contrast in the northern hemisphere remains controlled by the nature of vertical mixing even in the presence of Ekman transport (for negligible eddy transport). Saenko and Weaver [2003] assumed that the eddy transport is proportional to thermocline depth, a choice inspired by the scheme of *Gent and McWilliams* [1990]. For this representation of eddy-transport and with a stability-dependent κ_v, the MOC

decreases with increasing density contrast, provided that the eddy transport is below a threshold value. For stronger eddy transport, however, the more common response is obtained, i.e., the MOC increases with increasing density contrast. Thus, the contrasting equilibrium responses of the MOC for diferent natures of vertical mixing, which are obtained in this study, need to be examined with more complete models.

Acknowledgments. We thank Alain Colin de Verdière and Carl Wunsch for comments on the manuscript. Support for this work came from the U.S. National Science Foundation (authors CJ and OM), the 'Deutsche Forschungsgemeinschaft' (AP), the Swedish Science Research Council (JN), and the Swiss National Science Foundation (TFS).

REFERENCES

Bryden, H.L., and S. Imawaki, Ocean heat transport, G. Siedler, J. Church, and J. Gould (Eds.), *Ocean Circulation and Climate*, Volume 77 of *International Geophysical Series*, pp. 455-474. Academic Press, 2001.

Cummins, P.F., G. Holloway, and A.E. Gargett, Sensitivity of the GFDL ocean general circulation model to a parameterization of vertical diffusion, *J. Phys. Oceanogr.*, 20, 817-830, 1990.

Dijkstra, H.A. *Nonlinear physical oceanography: A dynamical system approach to the large scale ocean circulation and El Nino*. Springer, Dordrecht, New York, 2005.

Gargett, A.E., Vertical eddy diffusivity in the ocean interior, *J. Marine Res.*, 42, 359-393, 1984.

Gent, P.R., and J.C. McWilliams, Isopycnal mixing in ocean circulation models, *J. Phys. Oceanogr.*, 20, 150-155, 1990.

Gent, P.R., J. Willebrand, T.J. McDougall, and J.C. McWilliams, Parameterizing eddy-induced tracer transports in ocean circulation models, *J. Phys. Oceanogr.*, 25, 463-474, 1995.

Gnanadesikan, A., A simple predictive model for the structure of the oceanic thermocline, *Science*, 283, 2077-2079, 1999.

Hu, D., On the sensitivity of thermocline depth and meridional heat transport to vertical diffusivity in OGCMs, *J. Phys. Oceanogr.*, 26, 1480-1494, 1996.

Huang, R.X., Mixing and energetics of the ocean thermohaline circulation, *J. Phys. Oceanogr.*, 29, 727-746, 1999.

Kato, H., and O.M. Phillips, On the penetration of a turbulent layer into a stratified fluid, *J. Fluid Mech.*, 37, 643-655, 1969.

Klinger, B.A., and J. Marotzke, Behavior of double-hemisphere thermohaline flows in a single basin, *J. Phys. Oceanogr.*, 29, 382-399, 1999.

Marotzke, J., 1989. Instabilities and multiple steady states of the thermohaline circulation. in D.L.T. Anderson and J. Willebrand (Eds.), *Ocean Circulation Models: Combining Data and Dynamics*, NATO ASI, pp. 501-511. Kluwer.

Mohammad, R., and J. Nilsson, The role of diapycnal mixing for the equilibrium response of the thermohaline circulation, *Ocean Dynamics*, 54, 54-65, 2004.

Mohammad, R., and J. Nilsson, Symmetric and asymmetric modes of the thermohaline circulation, *Tellus*, *Ser. A*, 58, 616-627, 2006.

Munk, W., and C. Wunsch, Abyssal recipes II: Energetics of tidal and wind mixing, *Deep Sea Res.*, 45, 1977-2010, 1998.

Nilsson, J., G. Broström, and G. Walin, The thermohaline circulation and vertical mixing: Does weaker density stratification give stronger overturning?, *J. Phys. Oceanogr.*, 33, 2781-2795, 2003.

Nilsson, J., and G. Walin, Freshwater forcing as a booster of the thermohaline circulation, *Tellus*, 53A, 629-641, 2001.

Olsen, S.M., G. Shaffer, and C.J. Bjerrum, Ocean oxygen isotope constraints on mechanisms for millennial-scale climate variability, *Paleoceanography*, 20, doi:10.1029/2004PA001063, 2005.

Osborn, T.R., Estimates of the local rate of vertical diffusion from dissipation measurements, *J. Phys. Oceanogr.*, 10, 83-89, 1980.

Park, Y.-G., and K. Bryan, Comparison of thermally driven circulations from a depth-coordinate model and a isopycnal-layer model. Part I: Scaling-law sensitivity to vertical diffusivity, *J. Phys. Oceanogr.*, 31, 972-991, 2001.

Paul, A., and M. Schulz. Holocene climate variability on centennial-to-millennial time scales: 2. Internal and forced oscillations as possible causes, G. Wefer, W. Berger, K.-E. Behre, and E. Jansen (Eds.), *Climate Development and History of the North Atlantic Realm*, pp. 55-73. Springer-Verlag, Berlin, 2002.

Pedlosky, J. *Geophysical Fluid Dynamics* (2 ed.). Springer, 1987. 710 pp.

Polzin, K.L., J.M. Toole, and R.W. Schmitt, Finescale parameterizations of turbulent dissipation, *J. Phys. Oceanogr.*, 25, 306-328, 1995.

Saenko, O.A., and A.J. Weaver, Southern ocean upwelling and eddies: Sensitivity of the global overturning to the surface density range, *Tellus*, *Ser. A*, 55A, 106-111, 2003.

Samelson, R.M., and G.K. Vallis, Large-scale circulation with small diapycnal diffusion: The two-thermocline limit, *J. Marine Res.*, 55, 223-275, 1997.

Stoker, J.J., *Nonlinear vibrations*, Pure and applied mathemathics. Interscience publishers, Inc., New York, 1950. 273 pp.

Stommel, H., Thermohaline convection with two stable regimes of flow, *Tellus*, 13, 224-241, 1961.

Toggweiler, J.R., and B. Samuels, On the ocean's large-scale circulation near the limit of no vertical mixing, *J. Phys. Oceanogr.*, 28, 1832-1852, 1998.

Vallis, G.K., Large-scale circulation and production of stratification: Effects of wind, geometry, and diffusion, *J. Phys. Oceanogr.*, 30, 933-954, 2000.

Welander, P., 1986. Thermohaline effects in the ocean circulation and related simple models. in J. Willebrand and D.L.T. Anderson (Eds.), *Large-Scale Transport Processes in Oceans and Atmosphere*, pp. 163-200. D. Reidel.

Winton, M., and E.S. Sarachik, Thermohaline oscillations induced by strong steady salinity forcing of ocean general circulation models, *J. Phys. Oceanogr.*, 23, 1389-1410, 1993.

Wright, D.G., and T.F. Stocker, A zonally averaged ocean model for the thermohaline circulation, Part I: Model development and flow dynamics, *J. Phys. Oceanogr.*, 21, 1713-1724, 1991.

Wright, D.G., and T.F. Stocker, Sensitivities of a zonally averaged global ocean circulation model, *J. Geophys. Res.*, 97, 12,707-12,730, 1992.

Wright, D.G., T.F. Stocker, and D. Mercer, Closures used in zonally averaged ocean models, *J. Phys. Oceanogr.*, 28, 791-804, 1998.

Wright, D.G., C.B. Vreugdenhil, and T.M. Hughes, Vorticity dynamics and zonally averaged ocean circulation models, *J. Phys. Oceanogr.*, 25, 2141-2154, 1995.

Wunsch, C., and R. Ferrari, Vertical mixing, energy, and the general circulation of the oceans, *Ann. Rev. Fluid Mech.*, 36, 281-313, 2004.

C. Jackson, Institute of Geophysics, University of Texas at Austin, Austin, Texas, USA.

O. Marchal, Woods Hole Oceanographic Institution, Department of Geology/Geophysics, Quissett Campus, Clark Building, MS# 23, Woods Hole, Massachusetts 02543, USA. (omarchal@whoi.edu)

J. Nilsson, Department of Meteorology, University of Stockholm, Stockholm, Sweden.

A. Paul, Department of Geosciences, University of Bremen, Bremen, Germany.

T. F. Stocker, Climate and Environmental Physics Division, Physics Institute, University of Bern, Bern, Switzerland.